https://doi.org/10.48048/tis.2024.8537

Influence of Layer's Annealing Temperature on Sensing Properties of Spin-Coated SBS Layer Exposed to Alcohol Vapor

Tyas Nurul Zafirah[1,2], Masruroh[1], Istiroyah[1] and Setyawan Purnomo Sakti[1,2,*]

[1]*Department of Physics, Brawijaya University, Malang, Indonesia*
[2]*Sensor Technology Laboratory, Department of Physics, Brawijaya University, Malang, Indonesia*

([*]Corresponding author's e-mail: sakti@ub.ac.id)

Received: 6 June 2024, Revised: 24 June 2024, Accepted: 1 July 2024, Published: 20 October 2024

Abstract

QCM-based alcohol vapor sensors have been widely researched, and various materials have been deposited onto the sensor surface to serve as a functional layer. However, non-conductive polymers such as SBS as a functional layer for alcohol sensors are still minimally reported. In this study, the SBS was deposited on 1 side of the QCM using the spin coating technique. After deposition, the layer was annealed for 1 h. The annealing temperatures are 100, 150 and 200 °C. The concentrations of exposed alcohol vapor were 5, 10, 15, 20, 25, 50, 75 and 100 ppm. This study demonstrated that the SBS layer has the potential to be a functional layer of alcohol sensors. SBS 200 °C is an optimum functional layer for alcohol vapor sensors due to its high Δf and sensitivity. Meanwhile, SBS 100 °C has poor Δf and sensitivity. This is due to the morphology of 200 °C SBS, which consists of more valleys that perform as interaction sites for SBS and alcohol molecules. However, one of the limitations of SBS as a functional sensor layer for alcohol sensors is its low selectivity, which is a characteristic of rubbery polymers.

Keywords: Alcohol vapor, QCM, SBS, Sensor

Introduction

Alcohol is one of the VOCs present in household products. Alcohol-containing household products include hand sanitizers, detergents, perfumes, hair products, insect repellents, and so on [1-6]. Continuous alcohol exposure affects human health, causing hypoglycemia, cancer, respiratory problems, and even death [3,7-10]. As a result, sensors are required to monitor alcohol concentration in the air. Alcohol sensors have been developed using mass spectrometry (GCMS) [6,11,12], optical sensors [13-15], and acoustic sensors [16-18]. In this study, the alcohol sensor is an acoustic sensor with the advantages of real-time measurement, a rapid response time, and can operate at room temperature [19,20].

Quartz Crystal Microbalance (QCM)-based alcohol vapor sensors have been widely researched by depositing various materials as the functional layer of the sensor, including polyvinyl acetate [17], MOF [21], polyvinylpyrrolidone [22], chitosan [23], etc. Conductive polymers are widely used as functional layers for vapor/gas sensors [24-27]. This is due to its high sensitivity to VOCs, short response time, and cheap fabrication costs. However, due to the doping process during polymerization, this polymer has low stability and is sensitive to temperature and humidity changes [28-32]. Because conductive polymers have limitations, non-conductive polymers can be an alternative as a functional layer. Non-conductive polymers have better reproducibility and selectivity than conductive polymers, operate at room temperature, and have the ability to interact with certain types of gas, especially aromatic compounds [28,33-36].

Poly(styrene-block butadiene-block styrene) (SBS) is a thermoplastic elastomer composed of 2 polymers with distinct properties. Polystyrene (PS) is a glassy polymer; its chains are stiff. Meanwhile, polybutadiene (PB) is a rubbery polymer. Combining these 2 polymers gives SBS good durability due to the PS chain and high reversibility due to the PB chain [37-42]. SBS is commonly used in vehicle wheels, shoe soles, and asphalt mixtures. Adding SBS to asphalt increases strength and improves abrasion resistance [43-46]. Aside from that, SBS can be used as an additional material/filler in composites. The addition of SBS can improve sensor stability and sensitivity [47-50]. Meanwhile, SBS as a single material for the functional layer of the sensor is still rarely reported [51].

Annealing is a procedure to heat a material to a specific temperature and period and then cool it to room temperature to modify its properties. The annealing process in polymers is intended to relieve internal stress in polymer chains due to the deposition process. The annealing process in amorphous polymers provides enough energy for the polymer chains to organize themselves, increasing the unoccupied volume between the chains [52-57]. The amount of unoccupied volume can influence the number of alcohol molecules interacting with the layer. This may have an impact on sensor performance.

Although non-conductive polymers have several advantages over conductive polymers, limited studies have been conducted regarding applying non-conductive polymers as functional layers. Thus, the main objective of this study is to investigate the ability of SBS, a non-conductive polymer, to be utilised as a functional layer for QCM-based alcohol sensors. According to several previous studies, SBS has the advantage of high sensitivity. Thus, it can potentially be utilized as a functional layer for sensors. Furthermore, observations were made regarding the effect of SBS annealing temperature on layer morphology. These morphological differences are speculated to influence sensor performance.

Materials and methods

QCM 10 MHz with gold electrodes obtained from Shenzen Renlux Crystal Co. Ltd.,. Poly(styrene-block butadiene-block styrene) (SBS) 30 wt% styrene (Mw: 1.4×10^5 g/mol; CAS: 9003-55-8) from Sigma Aldrich. The organic solvents toluene (CAS: 108-88-3), methanol (CAS: 67-56-1), ethanol (CAS: 64-17-5), and 2-propanol (CAS: 67-63-0) with a purity of 99.9 % were bought from Merck.

SBS deposition on 1 side of the QCM was carried out using the spin coating technique. A specific mass of SBS dissolved in toluene solvent to produce solution concentrations of 1, 3 and 5 wt%. The spin coating settings are V = 50 µL, t_1 = 5s, ω_1 = 500 rpm, t_2 = 60s, and ω_2 = 3,000 rpm. After deposition, the SBS layer was annealed for 1 h. The annealing temperatures are 100, 150 and 200 °C. The objective of selecting these 3 temperatures was to observe the effect of temperature on the morphology of the SBS. The QCM/SBS is then exposed to alcohol vapor (methanol, ethanol, and 2-propanol) in a closed chamber [58]. The duration of the VOC exposure was set to 600 s. The concentrations of exposed alcohol vapor were 5, 10, 15, 20, 25, 50, 75 and 100 ppm. The layer characterization was done using Scanning Electron Microscopy (SEM) FEI-Quanta FEG 650 and Topography Measurement System TopMap µ.Lab TMS-1200 Polytec.

Results and discussion

SBS layer's characterization

The deposited SBS thickness (h) on the QCM sensor's surface is calculated by evaluating sensor frequencies before and after SBS deposition [59]. The thickness of the deposited SBS layer ranges from 39.4 to 355.1 nm (**Table 1**). The factor determining the thickness of the deposited layer using the spin coating technique is the concentration of the polymer solution [60,61]. The polymer layer is thicker as the solution concentration increases. Varying the concentration of the SBS solution from 1 to 5 wt% increases

layer thickness up to 800 %. This suggests that changes in solution concentration can effectively control the thickness of the SBS layer deposited by the spin coating technique.

Table 1 The effect of annealing temperature on the average roughness (Sa) and the effect of solution concentration on layer thickness (h).

T (°C)	wt%	Sa (nm)	h (nm)
100	SBS 1 %	570.53 ± 24.32	39.4
	SBS 3 %	640.63 ± 24.98	155.5
	SBS 5 %	662.64 ± 43.14	336.2
150	SBS 1 %	627.03 ± 19.53	47.6
	SBS 3 %	639.89 ± 7.54	122.4
	SBS 5 %	687.49 ± 15.09	355.1
200	SBS 1 %	516.82 ± 10.61	41.4
	SBS 3 %	631.30 ± 34.03	155.4
	SBS 5 %	602.87 ± 51.65	345.5

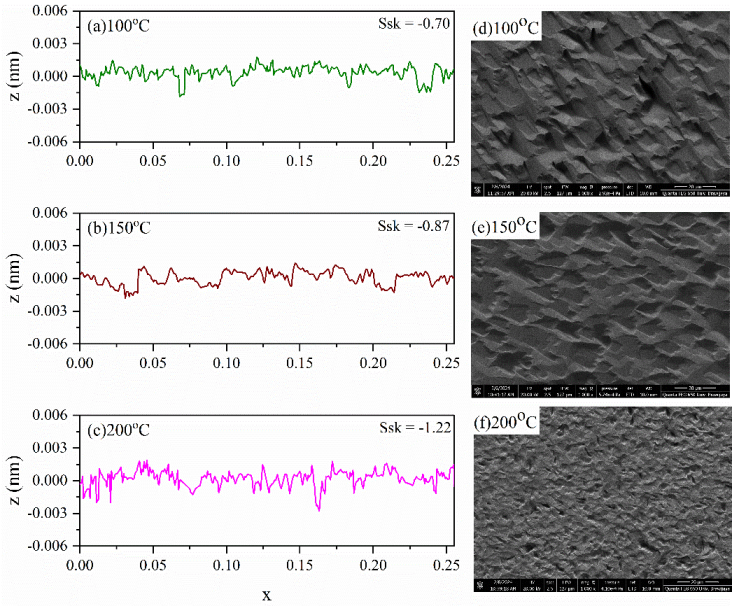

Figure 1 Characterization of SBS 5 %. (a), (b), (c) line profile of SBS layer surface and (d), (e), (f) SEM characterization.

SEM examination reveals that the annealing temperature influences the layer morphology (**Figure 1**). The higher annealing temperature causes the SBS layer to have more valleys with a smaller diameter. TMS characterization results support this as well. The TMS line profile demonstrates that the annealing temperature influences layer morphology. In addition, the roughness parameter measured with TMS is Ssk. The negative Ssk indicates that the layers have more valleys rather than hills. This is consistent with the SEM results, which show that the 200 °C SBS layer contains the most valleys. Moreover, the Sa parameter shows the same pattern. Sa will become rougher due to the increase in annealing temperature. The rougher SBS surface is expected to improve sensor performance.

The presence of more energy (due to the annealing treatment) causes the SBS chains to move and arrange themselves in a more ordered pattern. However, the degree of order in the polymer chains will not be as high as in crystalline polymers. This is because SBS is not a crystalline polymer. The movement of the polymer chains becomes more regular, resulting in a constant distance between the chains. As a result, the layer morphology currently has valleys of relatively uniform distances and diameters.

Response to alcohol vapor

In this study, the sensor response is expressed as a frequency shift of QCM (Δf). QCM is a mass sensor that operates following the Sauerbrey equation; thus, the additional mass on the sensor is proportional to Δf [62]. **Figure 2(a)** depicts the frequency pattern formed by SBS 100 °C with various thicknesses (SBS 1 - 5 wt%) exposed to ethanol with concentration of 5 - 100 ppm. At exposure of 10 ppm alcohol, layer thickness influences the sensor's response. QCM sensors with the thickest SBS layers exhibit the highest Δf. This is because this layer has the most interaction sites. As a result, more alcohol molecules engage with the layer. **Figures 2(b) - 2(d)** shows the Δf of SBS 5 % with different morphology (due to annealing temperature) for 3 types of alcohol at concentrations ranging from 5 - 100 ppm. SBS 5 % exhibits the most significant response to alcohol (**Figure 1(a)**). The Δf for the 3 alcohols follows the same pattern; layers annealed at higher temperatures exhibit a more significant response. This is because the SBS morphology grows more valley as the annealing temperature rises. The influence of the layer's annealing temperature on the sensor response appears significant, especially at higher alcohol concentrations (**Figures 2(b) - 2(d)**). At 25 ppm methanol, the annealing temperature increasing from 100 to 150 °C causes Δf to increase by 35.78 and 116.60 Hz for 150 to 200 °C. Meanwhile, at 100 ppm methanol, the sensor response increased significantly, up to 76.27 Hz (100 to 150 °C) and 122.40 Hz (150 to 200 °C). The sensor response to ethanol increased 145 and 54.8 % for 2-propanol due to the SBS layer's different morphology. Thus, it can be stated that the annealing temperature of the SBS layer significantly affects the QCM sensor's response.

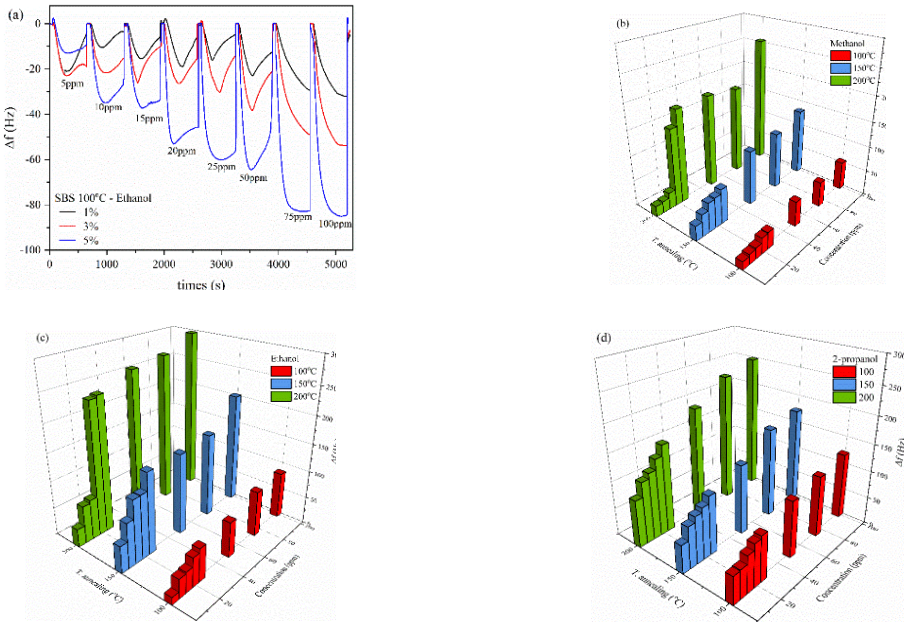

Figure 2 (a) Response curve of the SBS 100 °C exposed to 5 - 100 ppm ethanol. The effect of annealing temperature on the Δf of the sensor after exposure to (b) methanol, (c) ethanol, and (d) 2-propanol 5 - 100 ppm.

Based on Δf, SBS 200 °C has the best response due to the presence of the most valleys. This suggests that each valley can interact with only 1 alcohol molecule. At annealing temperatures of 100 and 150 °C, the SBS layer has valleys larger than SBS 200 °C. If each valley can interact with more than 1 alcohol molecule, the layer's annealing temperature should not affect the sensor response. Thus, the Langmuir model was used to prove this phenomenon. According to the Langmuir model, each site can interact with a single analyte molecule [23]. Fitting data show that the interactions between SBS and the 3 types of alcohol follow the Langmuir model (**Figure 3**). This is supported by the R^2 parameter, which is close to one. This explains why SBS 200 °C has the highest response.

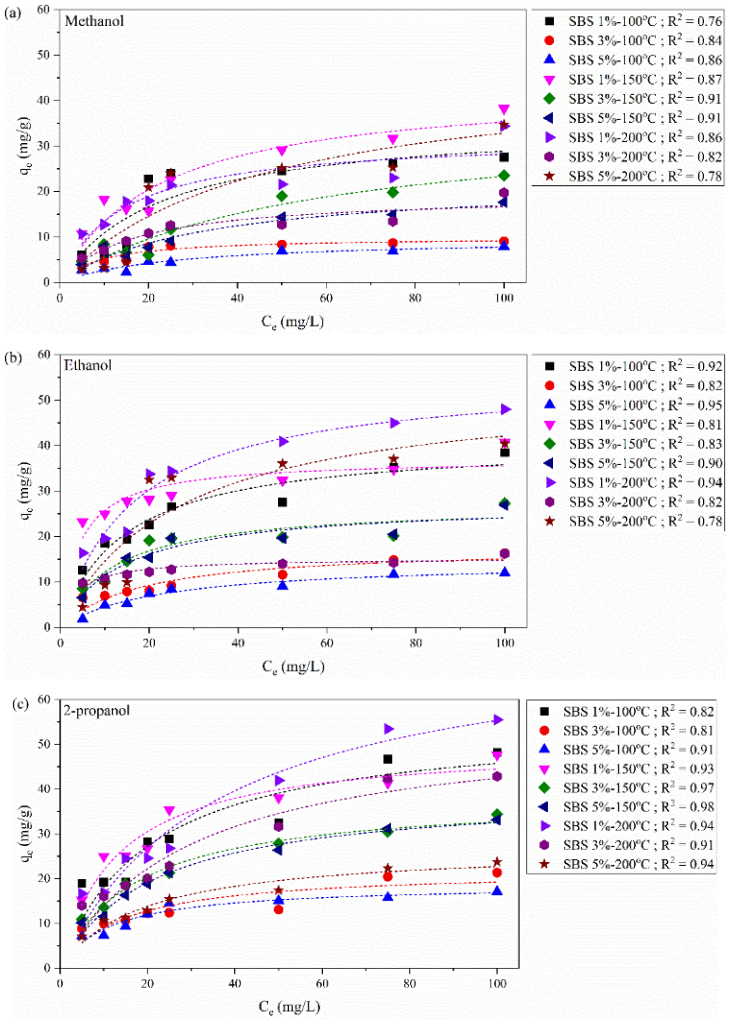

Figure 3 Data fitting using the Langmuir model on the response of SBS to (a) methanol, (b) ethanol, and (c) 2-propanol.

Response time

Figure 4 depicts the sensor's response time to 50 ppm alcohol. This concentration is in the middle range. At higher concentrations, it is hard to see the effect of SBS morphology on sensor response time because it approaches the end of the measurement (600 s). Response time is the required time of a sensor to detect an analyte with a specific concentration in a system [63]. The sensor response time is 4 - 61 % longer as the SBS annealing temperature rises from 100 to 200 °C. This condition occurs when SBS

interacts with the 3 types of alcohol. These findings suggest that the morphology of the SBS layer has a significant effect on sensor response time. The previous discussion stated that each interaction site can only interact with 1 alcohol molecule. SBS 200 °C has the most valley/interaction sites (according to SEM and TMS data). As a result, the layer takes longer to interact with the alcohol molecules.

Methanol, ethanol, and 2-propanol are homologous series alcohols. Methanol is the 1st homologous series of alcohols because it has 1 carbon atom. Ethanol has 2 carbon atoms and thus belongs to the 2nd homologous series of alcohols. Meanwhile, 2-propanol is a secondary alcohol with 3 carbon atoms that belong to the 3rd homologous series. The increasing number of C atoms indicates that the molecule is larger (**Table 2**).

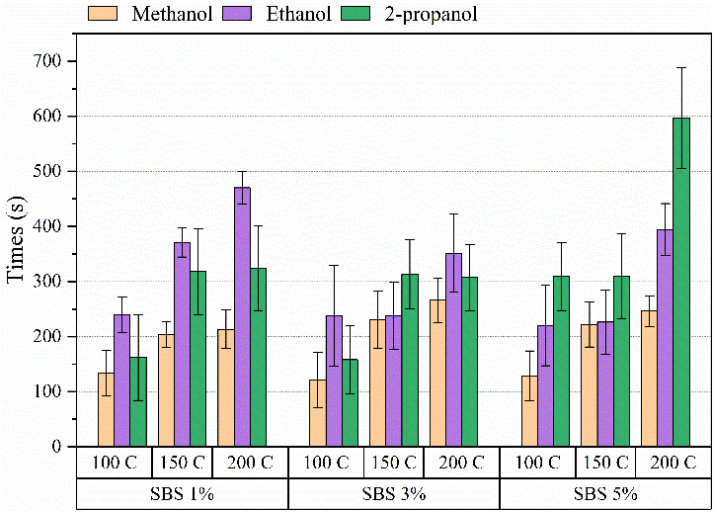

Figure 4 Response time of QCM/SBS exposed to 50 ppm alcohol vapor.

Table 2 Molecular size of alcohols [64].

No.	VOC	Diameter (Å)
1.	Methanol	3.80
2.	Ethanol	4.30
3.	2-propanol	4.70

Alcohol with a larger size causes the sensor's response time to be longer. This occurs in all 3 different SBS layer morphologies. Methanol has the smallest molecular size and can interact with the SBS layer in 121 - 266 s. Meanwhile, the response times for ethanol and 2-propanol are 220 - 470 and 158 - 597 s, respectively.

Sensitivity

Sensitivity (S) is another parameter for analyzing sensor performance. Sensitivity describes the sensor's ability to deliver output according to a given input. Sensor sensitivity was calculated from the slope of the sensor response to alcohol concentration [24,65]. The effect of SBS morphology on sensitivity follows the same pattern as the sensor response (Δf), with SBS 200 °C having the highest average sensitivity

compared to the other 2 annealing temperatures. This layer has the most interaction sites, allowing it to interact with more alcohol molecules than SBS 100 and 150 °C.

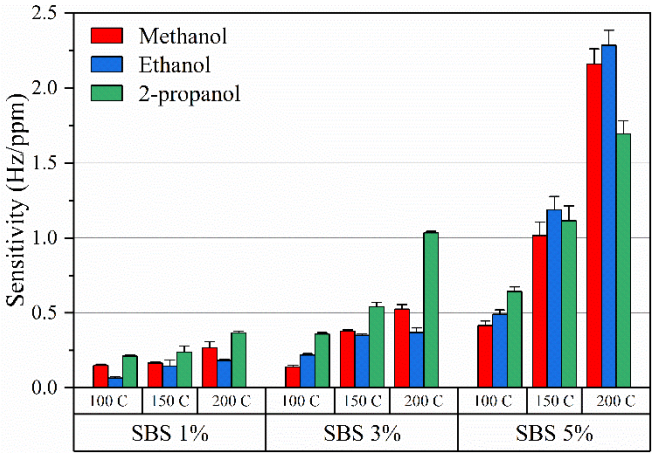

Figure 5 Sensitivity of SBS layer exposed to alcohols.

The sensor's sensitivity to methanol is 0.14 - 0.42 Hz/ppm for SBS 100 °C, 0.27 - 1.02 Hz/ppm for SBS 150 °C, and 0.16 - 2.16 Hz/ppm for SBS 200 °C (**Figure 5**). The sensitivity of SBS 200 °C is the highest compared to other annealing temperatures. The same pattern was observed in SBS sensitivity to ethanol and 2-propanol. SBS 200 °C has the highest sensitivity because it was based on response data (Δf). So, the sensor response and sensitivity will follow the same pattern. As a result, the sensor's sensitivity increases as the annealing temperature increases.

Partition coefficient

A layer's permeability and selectivity are indicated by the partition coefficient (K) [66-71]. Sensor selectivity is unaffected by layer morphology (**Figure 6**). No clear pattern indicates a correlation between layer morphology and partition coefficient. This is because SBS is a rubbery polymer. One of the disadvantages of rubbery polymers is their poor selectivity [72]. As a result, increasing the selectivity of the SBS functional layer will be more challenging.

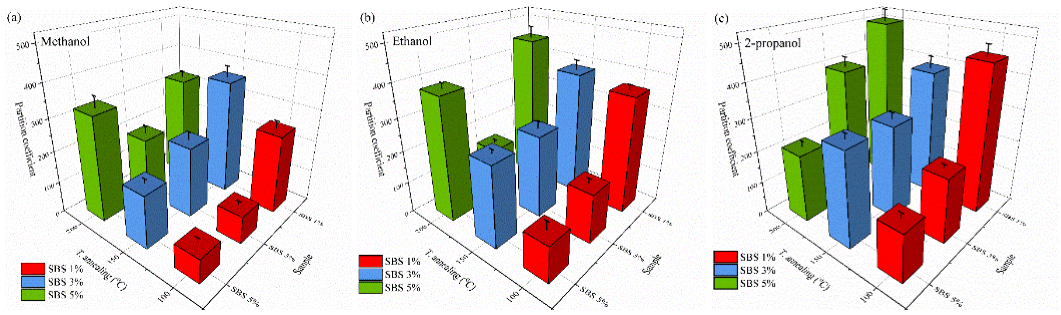

Figure 6 The partition coefficient of PS exposed to 100 ppm alcohol vapor.

Interaction SBS-alcohol

The desorption energy can determine the interaction type between alcohol and SBS. Unlike the adsorption process, where the activation energy is negligible (due to the low energy barrier), the desorption

process requires a specific barrier energy (the molar desorption energy, E_d), which must be greater or equal to the analyte-substrate interaction energy [73,74]. Physisorption occurs when the interaction energy between the analyte and the substrate is 10 - 40 kJ/mol [75]. According to **Table 3**, the interaction for the 3 types of alcohol is physisorption (Ed = 27 - 45 kJ/mol). Physisorption interactions are reversible. Alcohol molecules can be released from the SBS surface without changing the layer's properties. Thus, it can be concluded that SBS meets the requirements as a functional layer for alcohol vapor sensors because it can be used multiple times.

Table 3 Desorption energy of alcohol (100 ppm).

T. annealing (°C)	Sample	Desorption energy (kJ.mol^{-1})		
		Methanol	**Ethanol**	**2-propanol**
100	SBS 1 %	38.60	29.71	35.30
	SBS 3 %	39.19	36.32	36.78
	SBS 5 %	41.36	38.99	28.37
150	SBS 1 %	39.43	37.08	28.64
	SBS 3 %	41.33	36.52	27.51
	SBS 5 %	43.54	40.68	32.06
200	SBS 1 %	39.78	37.17	30.64
	SBS 3 %	41.80	38.01	33.34
	SBS 5 %	44.94	35.90	31.40

The interaction of alcohol molecules with SBS does not affect its properties. This is demonstrated by the sensor's impedance when exposed to methanol. In this study, SBS was deposited on the surface of the QCM sensor. Thus, changes in SBS properties can be determined by measuring the sensor's impedance when exposed to alcohol. The value and shape of the impedance curve can provide information about changes in layer properties. The thickest SBS (355.1 nm) was exposed to 5 mL methanol. The sensor impedance is measured before the exposure (expressed as t = 0), then the sensor is exposed to methanol for 10 min, with the sensor impedance measured every minute (expressed as t = 1 - 10 min). The exposure was stopped after 10 min (identical to the time used to measure the sensor response (Δf)). The sensor impedance was measured until it returned to its initial condition. Measurements are also performed every minute in this process (expressed as t = 11 min and so on).

The sensor frequency is also monitored during the impedance measurement process. This frequency can determine whether the methanol desorbs completely and the sensor has returned to its original state. **Figure 7** depicts the impedance curve of SBS after 5 mL of methanol exposure. At = 1 min, the sensor impedance does not change significantly ($\Delta Z = 4.063\Omega$), but the frequency does ($\Delta f = -349$ Hz). Interaction SBS-methanol causes the frequency changes. The frequency change is due to methanol molecules interacting with SBS. Apart from the impedance value, which remained constant, the impedance curve formed before and during exposure remains the same. The curve's shape is related to the layer's properties. It can be concluded that the interaction between alcohol molecules - SBS does not affect the layer's properties.

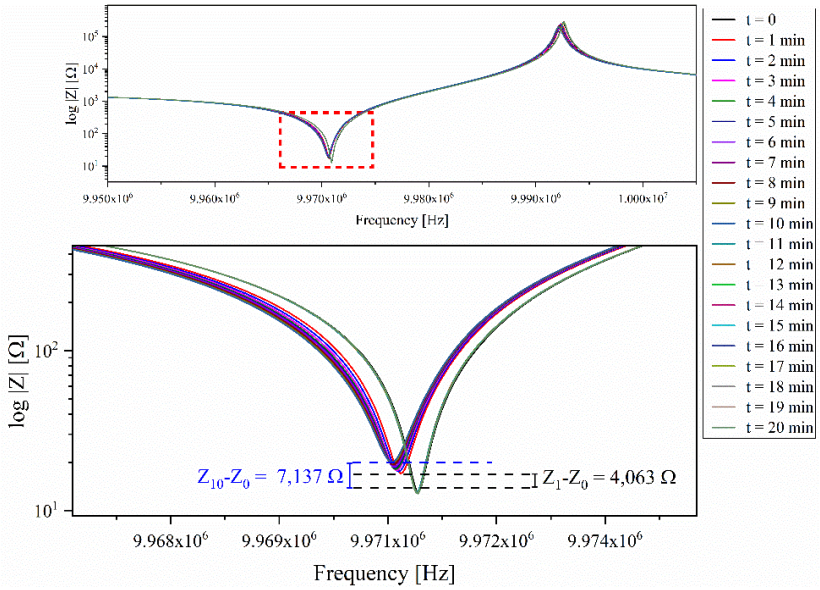

Figure 7 Impedance curve of SBS 5 % exposed to 5mL methanol.

SBS is undissolved in alcohol. According to the findings of this study, SBS can detect the presence of alcohol vapor in a closed system. According to the Hansen Solubility Parameter (HSP), SBS is not soluble in alcohol. SBS's insolubility in alcohol and its responses to alcohol show that it can be employed as an alcohol sensor. This is due to SBS's ability to meet sensor coating criteria, including high stability and chemically inert. As a result, sensors coated with this functional layer can be used repeatedly. SBS annealed at 200 °C is the optimum layer for an alcohol vapor sensor since it has high Δf and good sensitivity. Meanwhile, SBS 100 °C is undesirable for an alcohol vapor sensor because this layer has poor Δf and sensitivity (**Table 4**). The partition coefficient indicates that SBS has a poor sensitivity towards alcohol. This is one of the disadvantages of rubbery polymers. Further study is required to improve the SBS's selectivity. Several possible methods include the addition of other alcohol-selective materials to the SBS layer, surface activation such as UV irradiation or plasma treatment to produce certain functional groups that react with alcohol. Therefore, in the future, SBS layers with a high response, sensitivity, and selectivity to alcohol can be produced.

Table 4 Comparison of sensor performance based on 4 parameters.

T. annealing (°C)	Δf (Hz)	Response time (s)	Partition coefficient	Sensitivity (Hz.ppm^{-1})
100	13.04 - 121.54	121 - 309	74.23 - 453.13	0.14 - 0.64
150	29.44 - 202	204 - 371	165.69 - 388.34	0.14 - 1.69
200	20.63 - 296.97	213 - 597	153.1 - 502.41	0.16 - 2.28

In this study, the sensor was placed in a closed system and then exposed to alcohol. Meanwhile, in practice, the sensor may be placed in a room containing not only alcohol but also other VOCs (aromatics, ketones, ethers, and so on). Thus, it is necessary to consider and observe how SBS interacts to other VOCs. Specific patterns can be obtained that distinguish the interactions of SBS with alcohol from SBS with other VOCs. This information may be processed further using Artificial Intelligence.

Conclusions

This research demonstrated that annealing temperature influences layer morphology. The SBS layer has more valleys when annealed at a higher temperature. This is proved by the characterisation using SEM and TMS. Layer morphology influences the sensor's interaction with methanol, ethanol and 2-propanol. This study examined 4 sensor parameters: Sensor response (Δf), response time, partition coefficient, and sensitivity. Layer morphology does not affect sensor selectivity (represented by the partition coefficient). Because SBS is a rubbery polymer, one of its disadvantages is its low selectivity. SBS layer annealed at 200 °C has a high Δf and sensitivity but longer response time. Meanwhile, SBS 100 °C has low Δf and sensitivity. This is due to the morphology of 200 °C SBS, which consists of more valleys that perform as interaction sites for SBS and alcohol molecules. Each interaction site can only interact with a single alcohol molecule. This is proved by fitting with the Langmuir model, where the R^2 parameter is close to 1. The impedance curve and value show that the interaction between SBS and alcohol does not affect the layer properties. The desorption energy shows that the interaction between SBS and methanol is physisorption.

Acknowledgments

This work was funded under the PTUPT Research Grant Scheme 2023 with contract number 708.25/UN10.C10/TU/2023.

References

[1] JV Ashurst and TM Nappe. Methanol Toxicity, StatPearls, Available at: https://www.ncbi.nlm.nih.gov/books/NBK482121, accessed March 2024.

[2] A Kramer, M Arvand, B Christiansen, S Dancer, M Eggers, M Exner, D Müller, NT Mutters, I Schwebke and D Pittet. Ethanol is indispensable for virucidal hand antisepsis: Memorandum from the alcohol-based hand rub (ABHR) Task Force, WHO Collaborating Centre on Patient Safety, and the Commission for Hospital Hygiene and Infection Prevention (KRINKO), Robert Koch Instit. *Antimicrob. Resist. Infect. Control* 2022; **11**, 93.

[3] P Rayar and S Ratnapalan. Pediatric ingestions of house hold products containing ethanol: A review. *Clin. Pediatr.* 2013; **52**, 203-9.

[4] A Heeley-Hill, S Grange, M Ward, A Lewis, N Owen, C Jordan, G Hodgson and G Adamson. Frequency of use of household products containing VOCs and indoor atmospheric concentrations in homes. *Environ. Sci. Process. Impacts* 2021; **23**, 699-713.

[5] E David and VC Niculescu. Volatile organic compounds (VOCs) as environmental pollutants: Occurrence and mitigation using nanomaterials. *Int. J. Environ. Res. Publ. Health* 2021; **18**, 13147.

[6] S Ramadanoğlu and M Yayla. Alcohol and volatile organic compounds (VOCs) detected in biological, industrial, cosmetic and food samples using an Headspace GC-MS method. *In*: Proceedings of the 41st FEBS Congress, Molecular and Systems Biology for a Better Life, Ephesus/Kuşadasi, Turkey. 2016.

[7] EKL Hon, A Leung, E Cheung, B Lee, M Tsang and A Torres. An overview of exposure to ethanol-containing substances and ethanol intoxication in children based on three illustrated cases. *Drugs Context* 2018; **6**, 1-5.

[8] AR Chavez, M Sweeney and P Akpunonu. A case of unintentional isopropanol poisoning via transdermal absorption delayed by weekly hemodialysis. *Am. J. Case Rep.* 2021; **22**, e934529.

[9] TY Chang, KH Huang, CS Liu and BY Bao. Exposure to indoor volatile organic compounds and hypertension among thin film transistor liquid crystal display workers. *Atmosphere* 2020; **11**, 718.

[10] X Zhou, X Zhou, C Wang and H Zhou. Environmental and human health impacts of volatile organic

compounds: A perspective review. *Chemosphere* 2023; **313**, 137489.

[11] A Korban, S Charapitsa, R Čabala, L Sobolenko, V Egorov and S Sytova. Advanced GC-MS method for quality and safety control of alcoholic products. *Food Chem.* 2021; **338**, 128107.

[12] R Epping and M Koch. On-site detection of volatile organic compounds (VOCs). *Molecules* 2023; **28**, 1598.

[13] SF Memon, R Wang, B Strunz, BS Chowdhry, JT Pembroke and E Lewis. A review of optical fibre ethanol sensors: Current state and future prospects. *Sensors* 2022; **22**, 950.

[14] A Pathak and C Viphavakit. A review on all-optical fiber-based VOC sensors: Heading towards the development of promising technology. *Sens. Actuators A* 2022; **338**, 113455.

[15] D Liu, R Kumar, F Wei, W Han, A Mallik, JH Yuan, S Wan, X He, Z Kang, F Li, C Yu, G Farrell, Y Semenova and Q Wu. High sensitivity optical fiber sensors for simultaneous measurement of methanol and ethanol. *Sens. Actuators B* 2018; **271**, 1-8.

[16] I Constantinoiu and C Viespe. Detection of volatile organic compounds using surface acoustic wave sensor based on nanoparticles incorporated in polymer. *Coatings* 2019; **9**, 373.

[17] A Rianjanu, K Triyana, DB Nugroho, A Kusumaatmaja and R Roto. Electrospun polyvinyl acetate nanofiber modified quartz crystal microbalance for detection of primary alcohol vapor. *Sens. Actuators A* 2020; **301**, 111742.

[18] J Huang and J Wu. Robust and rapid detection of mixed volatile organic compounds in flow through air by a low cost electronic nose. *Chemosensors* 2020; **8**, 73.

[19] X Qiao, X Zhang, Y Tian and Y Meng. Progresses on the theory and application of quartz crystal microbalance. *Appl. Phys. Rev.* 2016; **3**, 031106.

[20] NC Speller, N Siraj, KS Mccarter, S Vaughan and IM Warner. Sensors and actuators B: Chemical QCM virtual sensor array: Vapor identification and molecular weight approximation. *Sens. Actuators B* 2017; **246**, 952-60.

[21] A Aghakhani, F Mohamadi and J Ghadimi. Novel alcohol vapour sensor based on the mixed-ligand modified MOF-199 coated quartz crystal microbalance. *Int. J. Environ. Anal. Chem.* 2021; **101**, 1803-20.

[22] R Sukowati, YM Rohman, BH Agung, DA Hapidin, H Damayanti and K Khairurrijal. An investigation of the influence of nanofibers morphology on the performance of QCM-based ethanol vapor sensor utilising polyvinylpyrrolidone nanofibers active layer. *Sens. Actuators B* 2023; **386**, 133708.

[23] NLL Hekiem, AAM Ralib, MAM Hatta, FB Ahmad and NF Za'Bah. Study of adsorption isotherms in the detection of acetone and isopropyl alcohol using QCM sensor with chitosan sensing layer. *In*: Proceedings of the IEEE International Conference on Semiconductor Electronics (ICSE), Kuala Lumpur, Malaysia. 2022, p. 29-32.

[24] L Feng, L Feng, Q Li, J Cui and J Guo. Sensitive formaldehyde detection with QCM sensor based on PAAm/MWCNTs and PVAm/MWCNTs. *ACS Omega* 2021; **6**, 14004-14.

[25] MR Eslami and N Alizadeh. Ultrasensitive and selective QCM sensor for detection of trace amounts of nitroexplosive vapors in ambient air based on polypyrrole-Bromophenol blue nanostructure. *Sens. Actuators B* 2019; **278**, 55-63.

[26] X Liu, J Wang and J Hou. Repeatability and sensitivity of quartz crystal microbalance (QCM) sensor array modified with four sensitive materials. *Mater. Sci. Semicond. Process.* 2022; **147**, 106764.

[27] J Völkle, K Kumpf, A Feldner, P Lieberzeit and P Fruhmann. Development of conductive molecularly imprinted polymers (cMIPs) for limonene to improve and interconnect QCM and chemiresistor sensing. *Sens. Actuators B* 2022, **356**, 131293.

[28] SH Hosseini and AA Entezami. Conducting polymer blends of polypyrrole with polyvinyl acetate, polystyrene, and polyvinyl chloride based toxic gas sensors. *J. Appl. Polym. Sci.* 2003; **90**, 49-62.

[29] SW Chiu and KT Tang. Towards a chemiresistive sensor-integrated electronic nose: A review. *Sensors* 2013; **13**, 14214-47.

[30] MO Ansari, SA Ansari, MH Cho, SP Ansari, MS Abdel-wahab and A Alshahrie. *Conducting polymer nanocomposites as gas sensors*. Functional polymers. Springer, Germany, 2019, p. 911-40.

[31] S Pirsa. *Chemiresistive gas sensors based on conducting polymers. In*: M Ahmadi, R Ismail and S Anwar (Eds.). Handbook of research on nanoelectronic sensor modeling and applications. IGI Global, Hershey, Pennsylvania, 2017, p. 150-80.

[32] YC Wong, BC Ang, ASMA Haseeb, AA Baharuddin and YH Wong. Review-conducting polymers as chemiresistive gas sensing materials: A review. *J. Electrochem. Soc.* 2020; **167**, 037503.

[33] M Giordano, M Russo, A Cusano, G Mensitieri and G Guerra. Syndiotactic polystyrene thin film as sensitive layer for an optoelectronic chemical sensing device. *Sens. Actuators B* 2005; **109**, 177-84.

[34] B Wang, L Zhou and X Wang. Surface acoustic wave sensor for formaldehyde gas detection using the multi-source spray-deposited graphene/PMMA composite film. *Front. Mater.* 2023; **9**, 1-8.

[35] S Han, X Zhuang, W Shi, X Yang, L Li and J Yu. Poly(3-hexylthiophene)/polystyrene (P3HT/PS) blends based organic field-effect transistor ammonia gas sensor. *Sens. Actuators B* 2016; **225**, 10-5.

[36] K Zhang, H Zhang, W Li, Y Tian, S Li, J Zhao and Y Li. PtOEP/PS composite particles based on fluorescent sensor for dissolved oxygen detection. *Mater. Lett.* 2016; **172**, 112-5.

[37] JK Jeong and DC Lee. Solubility parameter of a SBS triblock copolymer. *Korea Polym. J.* 1996; **4**, 9-15.

[38] W Jia, JY Jeon, L Zhu, S Park, C Bae and H Lin. Gas transport characteristics of fluorinated polystyrene-*b*-polybutadiene-*b*-polystyrene (F-SBS). *J. Memb. Sci.* 2019; **591**, 117296.

[39] P Costa, C Silvia, JC Viana and SL Mendez. Extruded thermoplastic elastomers styrene-butadiene-styrene/carbon nanotubes composites for strain sensor applications. *Composites Part B* 2014; **57**, 242-9.

[40] K Kanny and TP Mohan. *5 - Rubber nanocomposites with nanoclay as the filler*. *In*: S Thomas and HJ Maria (Eds.). Progress in rubber nanocomposites. Woodhead Publishing, Cambridge, 2017, p. 153-77.

[41] GD Airey. Rheological properties of styrene butadiene styrene polymer modified road bitumens. *Fuel* 2003; **82**, 1709-19.

[42] B Qin, B Li, J Zhang, X Xie and W Li. Highly sensitive strain sensor based on stretchable sandwich-type composite of carbon nanotube and poly(styrene–butadiene-styrene). *Sens. Actuator A* 2020; **315**, 112357.

[43] Y He, T Zhang, M Zeng, H Duan, B Zhang and J Yu. Effect of acylhydrazone self-healing agents with different structures on the properties of SBS modified asphalt waterproofing membrane. *Constr. Build. Mater.* 2024; **426**, 136238.

[44] Z Liu, P Wang, Z Huang, R Ren and K Liu. Nano-micelle formation and aggregation in SBS-Modified asphalt induced by π-π interaction using molecular dynamics. *Mater. Des.* 2024; **237**, 112571.

[45] K Zhang, W Xie and Y Zhao. Deterioration mechanism of adhesion property for SBS modified asphalt in salt-freeze-thawing environment. *Int. J. Adhes. Adhes.* 2023; **126**, 103441.

[46] J Gou, F Liu, E Shang and J Xin. Enhancing the physical properties of styrene-butadiene-styrene (SBS)-modified asphalt through polyetheramine-functionalized graphene oxide (PEA-GO) composites. *Constr. Build. Mater.* 2024; **418**, 135426.

[47] W Li, Y Zhou, Y Wang, L Jiang, J Ma, S Chen and FL Zhou. Core-sheath fiber-based wearable strain

sensor with high stretchability and sensitivity for detecting human motion. *Adv. Electron. Mater.* 2021; **7**, 1-9.

[48] X Wang, S Meng, M Tebyetekerwa, Y Li, J Pionteck, B Sun, Z Qin and M Zhu. Highly sensitive and stretchable piezoresistive strain sensor based on conductive poly(styrene-butadiene-styrene)/few layer graphene composite fiber. *Composites Part A* 2018, **105**, 291-9.

[49] X Wang, S Meng, M Tebyetekerwa, W Weng, J Pionteck, B Sun, Z Qin and M Zhu. Nanostructured polyaniline/poly(styrene-butadiene-styrene) composite fiber for use as highly sensitive and flexible ammonia sensor. *Synth. Met.* 2017; **233**, 86-93.

[50] M Park, J Im, M Shin, Y Min, J Park, H Cho, S Park, MB Shim, S Jeon, DY Chung, J Bae, J Park, U Jeong and K Kim. Highly stretchable electric circuits from a composite material of silver nanoparticles and elastomeric fibres. *Nat. Nanotechnol.* 2012; **7**, 803-9.

[51] MG Buonomenna, G Golemme, CM Tone, MPD Santo, F Ciuchi and E Perrotta. Nanostructured poly(styrene-b-butadiene-b-styrene) (SBS) membranes for the separation of nitrogen from natural gas. *Adv. Funct. Mater.* 2012; **22**, 1759-67.

[52] W Yu, X Wang, X Yin, E Ferraris and J Zhang. The effects of thermal annealing on the performance of material extrusion 3D printed polymer parts. *Mater. Des.* 2023; **226**, 111687.

[53] Z Jiang, P Liu, HJ Sue and T Bremner. Effect of annealing on the viscoelastic behavior of poly(ether-ether-ketone). *Polymer* 2019; **160**, 231-7.

[54] AW Riggins, JH Yu and MD Dadmun. Increasing the isotropy of 3D printed poly(ether ether ketone) using a combination of bimodal polymer blends and post-process thermal annealing. *Addit. Manuf.* 2024; **84**, 104127.

[55] F Servadei, L Zoli, P Galizia, C Melandri, S Failla and D Sciti. Effect of annealing treatments on the mechanical behaviour of UHTCMCs prepared by mild polymer infiltration and pyrolysis. *Ceram. Int.* 2023; **49**, 10032-40.

[56] K Jirakittidul, D Limthin, S Mahithithummathorn and S Phaewchimphlee. Effects of annealing temperature and time on properties of thermoplastic polyurethane based on different soft segments/multi-walled carbon nanotube nanocomposites. *Polymers* 2023; **15**, 364.

[57] MLD Vona. *Annealing of polymer membranes BT - encyclopedia of membranes*. *In*: E Drioli, L Giorno (Eds.). Encyclopedia of membranes. Springer Berlin Heidelberg, Germany, 2016.

[58] TN Zafirah, Masruroh, Istiroyah, AO Triqadafi and SP Sakti. Frequency response of the polystyrene films coated on the quartz crystal microbalance to the chloroform vapors. *AIP Conf. Proc.* 2023; **2818**, 90003.

[59] SP Sakti, Masruroh, Istiroyah, DD Kamasi and TN Zafirah. Ultra thick polystyrene coating on quartz crystal microbalance sensor. *Mater. Today Proc.* 2021; **44**, 3217-20.

[60] N Sahu, B Parija and S Panigrahi. Fundamental understanding and modeling of spin coating process: A review. *Indian J. Phys.* 2009; **83**, 493-502.

[61] MD Tyona. A theoritical study on spin coating technique. *Adv. Mater. Res.* 2013; **2**, 195-208.

[62] G Sauerbrey. Verwendung von Schwingquarzen zur Wägung dünner Schichten und zur Mikrowägung. *Zeitschrift Für Physik* 1959; **155**, 206-22.

[63] B Abebe, HCA Murthy and E Amare. Summary on adsorption and photocatalysis for pollutant remediation: Mini review. *J. Encapsulation Adsorpt. Sci.* 2018; **08**, 225-55.

[64] TC Bowen, RD Noble and JL Falconer. Fundamentals and applications of pervaporation through zeolite membranes. *J. Memb. Sci.* 2004; **245**, 1-33.

[65] NT Vinh, VN Phan, MH Nam, AT Le and NV Quy. NO_2 gas sensor based on QCM coated with iron oxide nanorods. *Vietnam J. Sci. Tech.* 2020; **58**, 204-11.]

[66] VE Bochenkov and GB Sergeev. *Sensitivity, selectivity and stability of gas-sensitive metal-oxide nanostructures. In*: A Umar and YB Hahn (Eds.). Metal oxide nanostructures and their applications. American Scientific Publishers, California, 2010, p. 31-52.

[67] Y Dong, W Gao, Q Zhou, Y Zheng and Z You. Characterization of the gas sensors based on polymer-coated resonant microcantilevers for the detection of volatile organic compounds. *Anal. Chim. Acta* 2010; **671**, 85-91.

[68] M Rodríguez-Torres, V Altuzar, C Mendoza-Barrera, G Beltrán-Pérez, J Castillo-Mixcóatl and S Muñoz-Aguirre. Discrimination improvement of a gas sensors' array using high-frequency quartz crystal microbalance coated with polymeric films. *Sensors* 2020; **20**, 6972.

[69] JW Grate, A Snow, DS Ballantine, H Wohltjen, MH Abraham, RA Mcgill and P Sasson. Determination of partition coefficients from surface acoustic wave vapor sensor responses and correlation with gas-liquid chromatographic partition coefficients. *Anal. Chem.* 1988; **60**, 869-75.

[70] JW Grate, SN Kaganove and VR Bhethanabotla. Comparisons of polymer/gas partition coefficients calculated from responses of thickness shear mode and surface acoustic wave vapor sensors. *Anal. Chem.* 1998; **70**, 199-203.

[71] Y Fu and HO Finklea. Quartz crystal microbalance sensor for organic vapor detection based on molecularly imprinted polymers. *Anal. Chem.* 2003; **75**, 5387-93.

[72] VS Abhisha, VP Swapna and R Stephen. *Modern trends and applications of gas transport through various polymers*. Elsevier, Netherlands, 2018, p. 363-89.

[73] DSJ Ballantine, SJ Martin, AJ Ricco, GC Frye, H Wohltjen, RM White and ET Zellers. *Acoustic wave sensors: Theory, design, and physico-chemical applications.* Academic Press, Massachusetts, 1997.

[74] X Li, HF Guo and HM Chen. Determination of the activation energy for desorption by derivative thermogravimetric analysis. *Adsorpt. Sci. Tech.* 2006; **24**, 907-23.

[75] P Pourhakkak, A Taghizadeh, M Taghizadeh, M Ghaedi and S Haghdoust. *Fundamentals of adsorption technology. In*: M Ghaedi (Ed.). Adsorption: Fundamental processes and applications. Elsevier, Netherlands, 2021.